Supplementary Material

Automated Search for Optimal Surface Phases in Grand Canonical Ensemble Powered by Machine Learning

Dongxiao Chen[1], Cheng Shang[1,2], Zhi-Pan Liu[1,2,3]*

[1]Collaborative Innovation Center of Chemistry for Energy Material, Shanghai Key Laboratory of Molecular Catalysis and Innovative Materials, Key Laboratory of Computational Physical Science, Department of Chemistry, Fudan University, Shanghai 200433, China

[2]Shanghai Qi Zhi Institution, Shanghai 200030, China

[3]Key Laboratory of Synthetic and Self-Assembly Chemistry for Organic Functional Molecules, Shanghai Institute of Organic Chemistry, Chinese Academy of Sciences, Shanghai 200032, China

Table of Contents

1. The architecture of global neural network potential

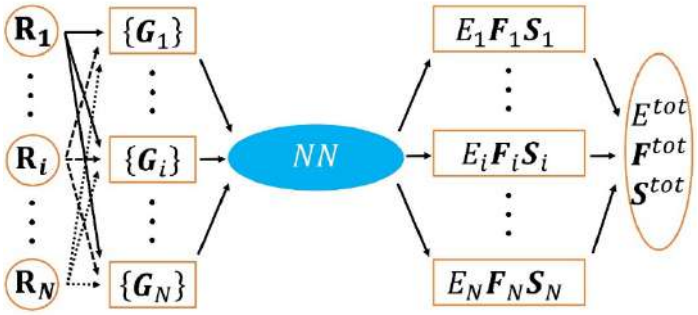

Scheme S1. Scheme of the HDNN architecture. The subscripts (1, *i*,…, *N*) are atom indices and represent the total atoms in a structure. The inputs of NN are a set of structural descriptors {***G***}, which are constructed from the Cartesian coordinates {**R**} of the structure, while the outputs of NN are the atomic properties { E_i, $\boldsymbol{F}_i$, $\boldsymbol{S}_i$ }, i.e., energies, forces, and stresses. The overall properties, E^{tot}, $\boldsymbol{F}^{tot}$, and $\boldsymbol{S}^{tot}$, can be calculated from the individual atomic contributions.

In this work, we utilized the high dimensional neural network (HDNN) scheme to construct the global NN (G-NN) potential, as shown in **Scheme S1**. The input nodes to NN are a set of structural descriptors of a structure, as discussed in our previous works.[1–3] The total energy E^{tot} of the structure can be composed as a linear combination of its atomic energy E^i from the output of NN

$$E^{tot} = \sum_i E_i \qquad \text{(S1)}$$

Consistently, the atomic force can be analytically derived from the total energy, i.e., the force component $F_{k,\alpha}$ (α = *x*, *y*, or *z*) acting on atom *k* is the derivative of the total energy E^{tot} with respect to coordinate $R_{k,\alpha}$. In combination with Eq. S1, the force component $F_{k,\alpha}$ then is related to the derivatives of the atomic energy E^i with respect to the j^{th} structural descriptors of atom *i*, $G_{j,i}$

$$F_{k,\alpha} = -\frac{\partial E^{tot}}{\partial R_{k,\alpha}} = -\sum_{i,j} \frac{\partial E_i}{\partial G_{j,i}} \frac{\partial G_{j,i}}{\partial R_{k,\alpha}} \qquad \text{(S2)}$$

Similarly, the element $\sigma_{\alpha\beta}$ of static stress tensor matrix can be analytically derived as

$$\sigma_{\alpha\beta} = -\frac{1}{V} \sum_{i,j,d} \frac{(\boldsymbol{r}_d)_\alpha (\boldsymbol{r}_d)_\beta}{r_d} \frac{\partial E_i}{\partial G_{j,i}} \frac{\partial G_{j,i}}{\partial r_d} \qquad \text{(S3)}$$

where $\boldsymbol{r}_d$ and r_d are the distance vector, constituted by $G_{j,i}$ and its module, respectively, and *V* is the volume of the structure.

2. SSW-NN simulation

2.1 SSW method

The stochastic surface walking (SSW) algorithm[4] has an automated climbing mechanism to manipulate a structure configuration from a minimum to a high-energy configuration along one random mode direction. The method was initially developed for aperiodic systems, such as molecules and clusters[5], and has been extended to periodic crystals[6].

The SSW method inherits the idea of bias-potential driven constrained-Broyden-dimer (BP-CBD) method for TS location[7]. In one particular SSW step a modified PES V, as shown in Eq. S4, is utilized for moving from the current minimum, $\mathbf{R}^m$ to a high energy configuration $\mathbf{R}^H$ by adding a series of bias Gaussian potential v_n (n=1...H). The bias potentials are added one by one consecutively along the direction $\mathbf{N}^n$ that defines the walking direction.

$$V = V_{real} + \sum_{n=1}^{H} v_n = V_{real} + \sum_{n=1}^{H} w_n \times \exp\left[-\left(\left(\boldsymbol{R} - \boldsymbol{R}^{n-1}\right)\cdot \boldsymbol{N}^n\right)^2/(2\times ds^2)\right] \quad \text{(S4)}$$

In the equation **R** is the current coordination vector of the structure and V_{real} represents the unmodified PES; $\mathbf{R}^n$ is the n^{th} local minima along the movement trajectory on the modified PES that is created after adding *n* Gaussian functions. The Gaussian function can be further controlled by its height *w* and its width *ds*. Once the maximum number of Gaussian functions (e.g. H=9) is reached, all bias potentials are removed and the local optimization is performed to quench the structure to a new minimum.

2.2 SSW-NN method

SSW-NN method is a machine-learning potential based global optimization method, which combines the global neural network (G-NN) potential with SSW method for fast and accurate global PES exploration as implemented in LASP code.[8] While traditional DFT calculations are frustrated for the global optimization of complex systems due to the high computational cost, SSW-NN method provides a general solution for PES scanning with both high efficiency and high accuracy.[9] The G-NN potential is trained based on DFT dataset and delivers a high speed of PES evaluation, ~4 orders of magnitude faster than DFT.[1–3] In our SSW-NN simulation for the surface oxides on Ag metal, the van der Waals correction was amended on G-NN PES by using D3 method with zero damping,[10,11] since it is important for accurately describing the behaviors of Ag surface oxides.[12]

2.3 Dataset generation and training of the initial Ag-C-H-O G-NN

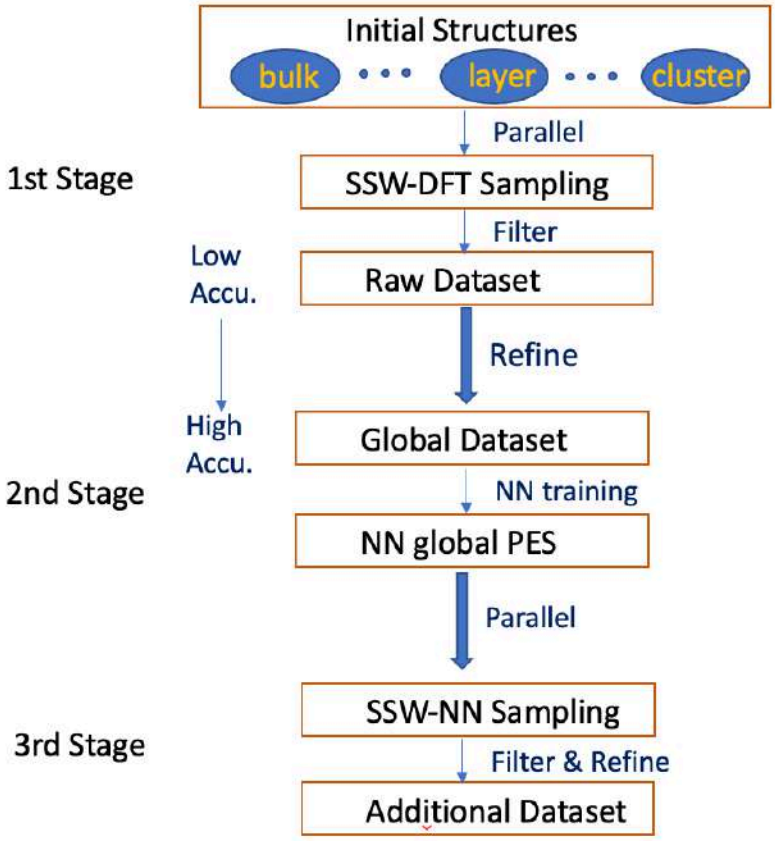

Scheme S2. Procedure for the generation of the global training dataset by SSW global optimization. In the first stage, the SSW sampling is typically performed by low accuracy DFT calculations. In the second stage, the global dataset is first refined with high accuracy DFT setups, and then a NN training is performed based on the accurate global dataset. In the third stage, an additional dataset is generated by SSW sampling utilizing the previously obtained NN PES, and is fed into the global dataset. A new cycle of NN training then starts based on the new global dataset (back to stage 2).

Before the ASOP simulation, an Ag-C-H-O G-NN potential is available from LASP G-NN library [13]. Now we briefly introduce the procedure to generate this initial G-NN potential.

The quality of the potential energy surface (PES) of G-NN is largely determined by its training dataset. We utilized the stochastic surface walking (SSW) global optimization to generate a global dataset, which is fully automated and does not need a priori knowledge on the system, such as the structural motif, e.g. bonding patterns and symmetry. The final obtained Ag-C-H-O global dataset contains a variety of structural patterns on the global PES, as summarized in **Table S1**. In brief, the SSW-NN method involves three stages to generate the global dataset (see **Scheme S2**), as described below.

(i) **The first stage** generates a raw dataset, which contains the most common atomic environment and serves to build an initial NN PES. This is done by performing density functional theory (DFT) SSW global optimization in a massively parallel way. In this stage, the DFT calculations have low accuracy set-ups and small unit cells to speed up the SSW search. By collecting and screening the structures from SSW trajectories, a raw dataset is obtained.

(ii) **The second stage** trains a NN global PES. This is done by refining the dataset using DFT calculations with high accuracy setups, followed by NN training on the accurate global dataset. The NN architecture applied in this stage utilizes a small set of structural descriptors and a small network size.

(iii) **The third stage** iteratively expands the global dataset. It targets to increase the predictive power of NN PES by incorporating more structural patterns into the dataset. This is done by performing SSW PES search using the NN PES obtained in the second stage, starting from a variety of initial structures. These initial structures are randomly constructed, and also include large systems with many atoms per unit cell. The structures from all the SSW trajectories are collected and filtered to generate an additional dataset. The new dataset is then fed to the global dataset to start a new cycle of NN training (back to stage 2).

Table S1. Structure information of the final dataset for G-NN training of Ag-C-H-O potential. Listed data are the number of the structures in the global dataset, as distinguished by the chemical formula, the number of atoms (Natoms), the type of structures (cluster, bulk, layer) and its total number (Ntotal).

Chemical Formula	Natoms	Ncluster	Nlayer	Nbulk	Ntotal
Ag14	14	0	3	30	33
Ag15	15	85	5	726	816
Ag16	16	0	1	6554	6555
Ag17	17	0	0	19	19
Ag28	28	0	0	34	34
Ag29	29	0	15	0	15
Ag30	30	0	31	32	63
Ag31	31	0	0	74	74
Ag32	32	0	2	93	95
Ag64	64	0	94	0	94
O1-Ag16	17	0	7	32	39
O1-Ag18	19	23	0	0	23
O1-Ag20	21	0	1	11	12
O1-Ag21	22	0	1	0	1
O1-Ag24	25	0	0	62	62
O2-Ag16	18	0	6	53	59
O2-Ag19	21	0	2	0	2
O2-Ag20	22	0	2	9	11
O2-Ag78	80	0	43	0	43

O3-Ag16	19	0	3	39	42
O3-Ag20	23	0	2	11	13
O3-Ag33	36	0	53	30	83
O3-Ag37	40	0	49	0	49
O4	4	0	15	0	15
O4-Ag16	20	0	6	54	60
O4-Ag24	28	0	0	32	32
O4-Ag76	80	0	48	0	48
O5-Ag8	13	0	1	64	65
O5-Ag35	40	0	31	0	31
O5-Ag76	81	0	12	0	12
O6-Ag4	10	0	0	2942	2942
O6-Ag8	14	0	0	23	23
O6-Ag16	22	0	1	78	79
O6-Ag30	36	0	47	97	144
O6-Ag34	40	0	101	0	101
O6-Ag68	74	0	33	0	33
O6-Ag72	78	0	60	0	60
O6-Ag75	81	0	5	0	5
O6-Ag76	82	0	9	0	9
O7-Ag8	15	0	0	1283	1283
O8-Ag6	14	97	0	0	97
O8-Ag8	16	105	5	3594	3704
O8-Ag16	24	0	18	99	117
O8-Ag24	32	66	0	82	148
O8-Ag28	36	0	73	9	82
O8-Ag70	78	0	28	0	28
O8-Ag72	80	0	26	0	26
O9-Ag8	17	0	0	46	46
O10-Ag8	18	0	5	288	293
O10-Ag16	26	0	1	43	44
O10-Ag24	34	0	0	29	29
O10-Ag72	82	0	10	0	10
O11	11	0	78	24	102
O11-Ag16	27	0	0	13	13
O11-Ag25	36	0	57	82	139
O11-Ag69	80	0	31	0	31
O11-Ag71	82	0	108	0	108
O11-Ag72	83	0	21	0	21
O12-Ag8	20	36	8	1171	1215
O12-Ag16	28	0	3	50	53
O12-Ag24	36	24	0	60	84
O12-Ag72	84	0	163	0	163
O12-Ag85	97	0	77	0	77
O12-Ag88	100	0	35	0	35
O14-Ag16	30	0	1	44	45
O15-Ag16	31	0	1	48	49
O15-Ag21	36	0	130	181	311
O15-Ag77	92	0	1	0	1
O16-Ag12	28	0	0	211	211
O16-Ag16	32	0	19	26	45
O16-Ag32	48	0	8	58	66
O18-Ag18	36	0	53	93	146
O18-Ag97	115	0	50	0	50
O20-Ag16	36	0	65	96	161

O22-Ag16	38	0	0	205	205
O24-Ag16	40	0	0	14	14
O35-Ag210	245	0	2	0	2
O36-Ag210	246	0	1	0	1
H1-Ag16	17	0	9	16	25
H1-O3-Ag32	36	0	48	0	48
H1-O5-Ag34	40	0	35	0	35
H1-O6-Ag29	36	0	45	46	91
H1-O8-Ag27	36	0	43	0	43
H1-O11-Ag24	36	0	35	37	72
H1-O13-Ag65	79	0	26	0	26
H1-O15-Ag20	36	0	73	98	171
H1-O18-Ag17	36	0	43	60	103
H1-O20-Ag15	36	0	45	41	86
H2-Ag16	18	0	3	240	243
H2-O1-Ag27	30	0	83	0	83
H2-O3-Ag31	36	0	64	0	64
H2-O6-Ag28	36	0	53	63	116
H2-O8-Ag26	36	0	53	0	53
H2-O11-Ag23	36	0	64	59	123
H2-O15-Ag19	36	0	122	102	224
H2-O18-Ag16	36	0	63	63	126
H2-O20-Ag14	36	0	57	52	109
H2-C1-O2-Ag16	21	0	63	1	64
H2-C1-O2-Ag27	32	0	81	1	82
H2-C2-O3-Ag27	34	0	185	12	197
H3-Ag16	19	0	74	174	248
H3-O3-Ag30	36	0	9	0	9
H3-O3-Ag34	40	0	26	0	26
H3-O6-Ag27	36	0	9	10	19
H3-O8-Ag25	36	0	9	0	9
H3-O11-Ag22	36	0	13	11	24
H3-O15-Ag18	36	0	16	16	32
H3-O18-Ag15	36	0	9	7	16
H3-O20-Ag13	36	0	12	8	20
H3-C1-O2-Ag18	24	0	49	1	50
H3-C2-O2-Ag32	39	0	2	0	2
H3-C2-O3-Ag23	31	0	2	0	2
H3-C2-O3-Ag24	32	0	35	0	35
H3-C2-O3-Ag27	35	0	18	0	18
H4-Ag12	16	1	0	0	1
H4-O3-Ag29	36	0	12	0	12
H4-O6-Ag26	36	0	16	10	26
H4-O8-Ag24	36	0	9	0	9
H4-O11-Ag21	36	0	13	12	25
H4-O15-Ag17	36	0	21	22	43
H4-O18-Ag14	36	0	12	10	22
H4-O20-Ag12	36	0	12	8	20
H4-C1-O2-Ag36	43	0	535	0	535
H4-C1-O3-Ag27	35	0	701	32	733
H4-C1-O3-Ag36	44	0	545	0	545
H4-C1-O3-Ag48	56	0	163	0	163
H4-C1-O4-Ag64	73	0	437	0	437
H4-C2-O1-Ag64	71	0	1486	0	1486
H4-C2-O2-Ag27	35	0	19	0	19

H4-C2-O3-Ag20	29	0	5	0	5
H4-C2-O4-Ag11	21	0	12	4	16
H4-C2-O4-Ag12	22	0	526	445	971
H4-C2-O4-Ag24	34	0	46	2	48
H4-C2-O4-Ag26	36	0	5	0	5
H4-C2-O4-Ag27	37	0	400	11	411
H4-C2-O4-Ag64	74	0	10	0	10
H4-C2-O5-Ag24	35	0	12	0	12
H4-C2-O6-Ag44	56	0	318	0	318
H4-C2-O6-Ag60	72	0	59	0	59
H4-C2-O6-Ag74	86	0	20	0	20
H4-C2-O6-Ag76	88	0	127	0	127
H4-C2-O7-Ag41	54	0	101	0	101
H4-C2-O7-Ag43	56	0	106	0	106
H4-C2-O8-Ag45	59	0	100	0	100
H4-C2-O8-Ag64	78	0	28	0	28
H4-C2-O8-Ag76	90	0	30	0	30
H4-C2-O10-Ag41	57	0	99	0	99
H4-C2-O10-Ag43	59	0	90	1	91
H4-C2-O10-Ag45	61	0	108	6	114
H4-C2-O11-Ag42	59	0	176	0	176
H4-C2-O11-Ag43	60	0	487	3	490
H4-C2-O11-Ag44	61	0	96	0	96
H4-C2-O11-Ag45	62	0	183	0	183
H4-C2-O11-Ag53	70	0	7	0	7
H4-C2-O12-Ag20	38	0	36	0	36
H4-C2-O12-Ag41	59	0	299	1	300
H4-C2-O12-Ag42	60	0	112	0	112
H4-C2-O12-Ag43	61	0	207	1	208
H4-C2-O12-Ag44	62	0	98	1	99
H4-C2-O12-Ag53	71	0	124	0	124
H4-C2-O12-Ag77	95	0	20	0	20
H4-C2-O12-Ag78	96	0	20	0	20
H4-C2-O12-Ag85	103	0	46	0	46
H4-C2-O12-Ag86	104	0	20	0	20
H4-C2-O13-Ag41	60	0	97	1	98
H4-C2-O13-Ag45	64	0	277	0	277
H4-C2-O16-Ag116	138	0	619	0	619
H4-C2-O20-Ag92	118	0	101	0	101
H4-C2-O20-Ag93	119	0	40	0	40
H4-C2-O20-Ag95	121	0	89	0	89
H4-C2-O20-Ag96	122	0	89	0	89
H4-C2-O32-Ag56	94	0	80	0	80
H4-C2-O36-Ag211	253	0	9	0	9
H6-C1-O1-Ag27	35	0	62	6	68
H6-C1-O2-Ag27	36	0	413	22	435
H6-C1-O3-Ag12	22	0	132	184	316
H6-C2-O2-Ag36	46	0	530	0	530
H6-C2-O3-Ag36	47	0	523	0	523
H6-C2-O3-Ag48	59	0	161	0	161
H6-C2-O4-Ag36	48	0	517	0	517
H6-C3-O1-Ag48	58	0	160	0	160
H6-C3-O1-Ag64	74	0	1000	0	1000
H8-Ag8	16	9	0	7	16
H8-O6-Ag58	72	0	39	0	39

H8-O12-Ag52	72	0	45	9	54
H8-O16-Ag48	72	0	50	0	50
H8-O22-Ag42	72	0	30	47	77
H8-O30-Ag34	72	0	21	108	129
H8-O36-Ag28	72	0	5	50	55
H8-O40-Ag24	72	0	35	6	41
H8-C1-O2-Ag27	38	0	1	0	1
H8-C2-O2-Ag23	35	0	7	1	8
H8-C2-O2-Ag24	36	0	8	4	12
H8-C3-O2-Ag48	61	0	1056	0	1056
H8-C3-O3-Ag48	62	0	1039	0	1039
H8-C4-O1-Ag26	39	0	1	0	1
H8-C4-O1-Ag27	40	0	1	0	1
H8-C4-O1-Ag32	45	0	7	0	7
H8-C4-O1-Ag33	46	0	6	0	6
H8-C4-O2-Ag24	38	0	8	0	8
H8-C4-O2-Ag25	39	0	1	0	1
H8-C4-O2-Ag26	40	0	1	0	1
H8-C4-O2-Ag32	46	0	8	0	8
H8-C4-O2-Ag33	47	0	6	0	6
H8-C4-O3-Ag24	39	0	11	0	11
H8-C4-O3-Ag25	40	0	9	0	9
H8-C4-O3-Ag26	41	0	3	0	3
H8-C4-O3-Ag27	42	0	15	0	15
H8-C4-O3-Ag32	47	0	10	0	10
H8-C4-O3-Ag33	48	0	9	0	9
H8-C4-O3-Ag34	49	0	1	0	1
H8-C4-O3-Ag35	50	0	3	0	3
H8-C4-O3-Ag36	51	0	5	0	5
H8-C4-O3-Ag37	52	0	10	0	10
H8-C4-O3-Ag38	53	0	19	0	19
H8-C4-O3-Ag39	54	0	14	0	14
H8-C4-O4-Ag24	40	0	17	0	17
H8-C4-O4-Ag25	41	0	25	0	25
H8-C4-O4-Ag26	42	0	20	0	20
H8-C4-O4-Ag27	43	0	28	0	28
H8-C4-O4-Ag30	46	0	4	0	4
H8-C4-O4-Ag31	47	0	9	0	9
H8-C4-O4-Ag32	48	0	7	0	7
H8-C4-O4-Ag33	49	0	11	0	11
H8-C4-O4-Ag34	50	0	3	0	3
H8-C4-O4-Ag35	51	0	2	0	2
H8-C4-O4-Ag36	52	0	3	0	3
H8-C4-O4-Ag37	53	0	21	0	21
H8-C4-O4-Ag38	54	0	26	0	26
H8-C4-O4-Ag39	55	0	9	0	9
H8-C4-O4-Ag42	58	0	2	0	2
H8-C4-O4-Ag43	59	0	8	0	8
H8-C4-O5-Ag30	47	0	2	0	2
H8-C4-O5-Ag31	48	0	11	0	11
H8-C4-O5-Ag32	49	0	15	0	15
H8-C4-O5-Ag33	50	0	24	0	24
H8-C4-O5-Ag34	51	0	15	0	15
H8-C4-O5-Ag35	52	0	9	0	9
H8-C4-O5-Ag36	53	0	7	0	7

H8-C4-O5-Ag37	54	0	22	0	22
H8-C4-O5-Ag38	55	0	15	0	15
H8-C4-O5-Ag39	56	0	16	0	16
H8-C4-O5-Ag42	59	0	1	0	1
H8-C4-O5-Ag43	60	0	8	0	8
H8-C4-O5-Ag46	63	0	7	0	7
H8-C4-O5-Ag47	64	0	7	0	7
H8-C4-O5-Ag48	65	0	9	0	9
H8-C4-O5-Ag53	70	0	1	0	1
H8-C4-O6-Ag32	50	0	8	0	8
H8-C4-O6-Ag33	51	0	14	0	14
H8-C4-O6-Ag34	52	0	1	0	1
H8-C4-O6-Ag35	53	0	1	0	1
H8-C4-O6-Ag36	54	0	14	0	14
H8-C4-O6-Ag37	55	0	35	0	35
H8-C4-O6-Ag38	56	0	24	0	24
H8-C4-O6-Ag39	57	0	16	0	16
H8-C4-O6-Ag40	58	0	2	0	2
H8-C4-O6-Ag41	59	0	1	0	1
H8-C4-O6-Ag42	60	0	7	0	7
H8-C4-O6-Ag43	61	0	5	0	5
H8-C4-O6-Ag44	62	0	5	0	5
H8-C4-O6-Ag45	63	0	4	0	4
H8-C4-O6-Ag46	64	0	6	0	6
H8-C4-O6-Ag47	65	0	7	0	7
H8-C4-O6-Ag48	66	0	18	0	18
H8-C4-O6-Ag49	67	0	8	0	8
H8-C4-O6-Ag53	71	0	2	0	2
H8-C4-O6-Ag57	75	0	6	0	6
H8-C4-O6-Ag58	76	0	3	0	3
H8-C4-O6-Ag75	93	0	20	0	20
H8-C4-O7-Ag32	51	0	9	0	9
H8-C4-O7-Ag33	52	0	11	0	11
H8-C4-O7-Ag34	53	0	2	0	2
H8-C4-O7-Ag35	54	0	5	0	5
H8-C4-O7-Ag36	55	0	10	0	10
H8-C4-O7-Ag37	56	0	27	0	27
H8-C4-O7-Ag38	57	0	27	0	27
H8-C4-O7-Ag39	58	0	5	0	5
H8-C4-O7-Ag40	59	0	4	0	4
H8-C4-O7-Ag41	60	0	5	0	5
H8-C4-O7-Ag42	61	0	11	0	11
H8-C4-O7-Ag43	62	0	8	0	8
H8-C4-O7-Ag44	63	0	13	0	13
H8-C4-O7-Ag45	64	0	13	0	13
H8-C4-O7-Ag46	65	0	5	0	5
H8-C4-O7-Ag47	66	0	13	0	13
H8-C4-O7-Ag48	67	0	20	0	20
H8-C4-O7-Ag49	68	0	18	0	18
H8-C4-O7-Ag50	69	0	1	0	1
H8-C4-O7-Ag52	71	0	5	0	5
H8-C4-O7-Ag53	72	0	3	0	3
H8-C4-O7-Ag56	75	0	4	0	4
H8-C4-O7-Ag57	76	0	8	0	8
H8-C4-O7-Ag58	77	0	16	0	16

H8-C4-O8-Ag32	52	0	13	0	13
H8-C4-O8-Ag33	53	0	6	0	6
H8-C4-O8-Ag35	55	0	2	0	2
H8-C4-O8-Ag36	56	0	14	0	14
H8-C4-O8-Ag37	57	0	6	0	6
H8-C4-O8-Ag40	60	0	5	0	5
H8-C4-O8-Ag41	61	0	6	0	6
H8-C4-O8-Ag43	63	0	6	0	6
H8-C4-O8-Ag44	64	0	7	0	7
H8-C4-O8-Ag45	65	0	11	0	11
H8-C4-O8-Ag46	66	0	16	0	16
H8-C4-O8-Ag47	67	0	12	0	12
H8-C4-O8-Ag48	68	0	16	0	16
H8-C4-O8-Ag49	69	0	17	0	17
H8-C4-O8-Ag51	71	0	5	0	5
H8-C4-O8-Ag53	73	0	4	0	4
H8-C4-O8-Ag54	74	0	2	0	2
H8-C4-O8-Ag55	75	0	9	0	9
H8-C4-O8-Ag57	77	0	6	0	6
H8-C4-O8-Ag58	78	0	2	0	2
H8-C4-O8-Ag62	82	0	6	0	6
H8-C4-O8-Ag63	83	0	7	0	7
H8-C4-O8-Ag96	116	0	20	0	20
H8-C4-O9-Ag40	61	0	3	0	3
H8-C4-O9-Ag41	62	0	5	0	5
H8-C4-O9-Ag45	66	0	7	0	7
H8-C4-O9-Ag47	68	0	20	0	20
H8-C4-O9-Ag48	69	0	15	0	15
H8-C4-O9-Ag50	71	0	4	0	4
H8-C4-O9-Ag51	72	0	5	0	5
H8-C4-O9-Ag53	74	0	3	0	3
H8-C4-O9-Ag54	75	0	4	0	4
H8-C4-O9-Ag55	76	0	13	0	13
H8-C4-O9-Ag57	78	0	8	0	8
H8-C4-O9-Ag58	79	0	11	0	11
H8-C4-O10-Ag45	67	0	23	0	23
H8-C4-O10-Ag53	75	0	4	0	4
H8-C4-O10-Ag54	76	0	3	0	3
H8-C4-O10-Ag55	77	0	9	0	9
H8-C4-O12-Ag87	111	0	20	0	20
H10-O5-Ag12	27	0	109	0	109
H11-Ag5	16	0	0	10	10
H11-O5-Ag12	28	0	54	2	56
H12-O5-Ag12	29	0	43	6	49
H12-C2-O4-Ag12	30	0	380	444	824
H12-C6-O4-Ag36	58	0	12	0	12
H12-C6-O4-Ag37	59	0	20	0	20
H12-C6-O4-Ag38	60	0	17	0	17
H12-C6-O5-Ag36	59	0	15	0	15
H12-C6-O5-Ag37	60	0	28	0	28
H12-C6-O5-Ag38	61	0	21	0	21
H12-C6-O5-Ag42	65	0	9	0	9
H12-C6-O5-Ag43	66	0	8	0	8
H12-C6-O5-Ag44	67	0	1	0	1
H12-C6-O5-Ag49	72	0	1	0	1

H12-C6-O5-Ag50	73	0	3	0	3
H12-C6-O5-Ag51	74	0	5	0	5
H12-C6-O6-Ag36	60	0	16	0	16
H12-C6-O6-Ag37	61	0	20	0	20
H12-C6-O6-Ag38	62	0	36	0	36
H12-C6-O6-Ag39	63	0	33	0	33
H12-C6-O6-Ag40	64	0	34	0	34
H12-C6-O6-Ag41	65	0	45	0	45
H12-C6-O6-Ag42	66	0	5	0	5
H12-C6-O6-Ag43	67	0	3	0	3
H12-C6-O6-Ag44	68	0	5	0	5
H12-C6-O6-Ag48	72	0	2	0	2
H12-C6-O6-Ag50	74	0	1	0	1
H12-C6-O6-Ag51	75	0	5	0	5
H12-C6-O6-Ag55	79	0	3	0	3
H12-C6-O6-Ag56	80	0	2	0	2
H12-C6-O6-Ag57	81	0	16	0	16
H12-C6-O6-Ag58	82	0	17	0	17
H12-C6-O6-Ag62	86	0	5	0	5
H12-C6-O6-Ag76	100	0	30	0	30
H12-C6-O7-Ag42	67	0	1	0	1
H12-C6-O7-Ag43	68	0	6	0	6
H12-C6-O7-Ag44	69	0	10	0	10
H12-C6-O7-Ag45	70	0	11	0	11
H12-C6-O7-Ag46	71	0	8	0	8
H12-C6-O7-Ag47	72	0	10	0	10
H12-C6-O7-Ag48	73	0	11	0	11
H12-C6-O7-Ag49	74	0	2	0	2
H12-C6-O7-Ag50	75	0	1	0	1
H12-C6-O7-Ag51	76	0	3	0	3
H12-C6-O7-Ag54	79	0	7	0	7
H12-C6-O7-Ag55	80	0	17	0	17
H12-C6-O7-Ag56	81	0	13	0	13
H12-C6-O7-Ag57	82	0	21	0	21
H12-C6-O7-Ag58	83	0	33	0	33
H12-C6-O7-Ag59	84	0	5	0	5
H12-C6-O7-Ag62	87	0	5	0	5
H12-C6-O7-Ag67	92	0	2	0	2
H12-C6-O8-Ag48	74	0	5	0	5
H12-C6-O8-Ag49	75	0	2	0	2
H12-C6-O8-Ag50	76	0	2	0	2
H12-C6-O8-Ag51	77	0	3	0	3
H12-C6-O8-Ag53	79	0	3	0	3
H12-C6-O8-Ag54	80	0	6	0	6
H12-C6-O8-Ag55	81	0	12	0	12
H12-C6-O8-Ag56	82	0	19	0	19
H12-C6-O8-Ag57	83	0	24	0	24
H12-C6-O8-Ag58	84	0	34	0	34
H12-C6-O8-Ag59	85	0	12	0	12
H12-C6-O8-Ag60	86	0	4	0	4
H12-C6-O8-Ag61	87	0	3	0	3
H12-C6-O8-Ag62	88	0	4	0	4
H12-C6-O8-Ag63	89	0	12	0	12
H12-C6-O8-Ag65	91	0	1	0	1
H12-C6-O8-Ag66	92	0	1	0	1

H12-C6-O8-Ag67	93	0	16	0	16
H12-C6-O8-Ag68	94	0	4	0	4
H12-C6-O9-Ag53	80	0	8	0	8
H12-C6-O9-Ag54	81	0	15	0	15
H12-C6-O9-Ag55	82	0	25	0	25
H12-C6-O9-Ag57	84	0	23	0	23
H12-C6-O9-Ag58	85	0	45	0	45
H12-C6-O9-Ag59	86	0	25	0	25
H12-C6-O9-Ag61	88	0	6	0	6
H12-C6-O9-Ag62	89	0	11	0	11
H12-C6-O9-Ag63	90	0	12	0	12
H12-C6-O9-Ag65	92	0	2	0	2
H12-C6-O9-Ag66	93	0	17	0	17
H12-C6-O9-Ag67	94	0	18	0	18
H12-C6-O9-Ag68	95	0	7	0	7
H12-C6-O9-Ag69	96	0	15	0	15
H12-C6-O9-Ag70	97	0	13	0	13
H12-C6-O9-Ag71	98	0	17	0	17
H12-C6-O9-Ag72	99	0	13	0	13
H12-C6-O10-Ag53	81	0	8	0	8
H12-C6-O10-Ag54	82	0	4	0	4
H12-C6-O10-Ag55	83	0	9	0	9
H12-C6-O10-Ag57	85	0	29	0	29
H12-C6-O10-Ag58	86	0	4	0	4
H12-C6-O10-Ag59	87	0	2	0	2
H12-C6-O10-Ag60	88	0	4	0	4
H12-C6-O10-Ag62	90	0	18	0	18
H12-C6-O10-Ag63	91	0	6	0	6
H12-C6-O10-Ag64	92	0	1	0	1
H12-C6-O10-Ag66	94	0	14	0	14
H12-C6-O10-Ag67	95	0	16	0	16
H12-C6-O10-Ag68	96	0	17	0	17
H12-C6-O10-Ag69	97	0	8	0	8
H12-C6-O10-Ag70	98	0	17	0	17
H12-C6-O10-Ag71	99	0	26	0	26
H12-C6-O10-Ag72	100	0	19	0	19
H12-C6-O11-Ag54	83	0	22	0	22
H12-C6-O11-Ag57	86	0	24	0	24
H12-C6-O11-Ag61	90	0	10	0	10
H12-C6-O11-Ag62	91	0	10	0	10
H12-C6-O11-Ag63	92	0	1	0	1
H12-C6-O11-Ag64	93	0	4	0	4
H12-C6-O11-Ag66	95	0	12	0	12
H12-C6-O11-Ag67	96	0	32	0	32
H12-C6-O11-Ag68	97	0	27	0	27
H12-C6-O11-Ag72	101	0	2	0	2
H12-C6-O12-Ag54	84	0	27	0	27
H12-C6-O12-Ag58	88	0	10	0	10
H12-C6-O12-Ag59	89	0	9	0	9
H12-C6-O12-Ag61	91	0	14	0	14
H12-C6-O12-Ag62	92	0	6	0	6
H12-C6-O12-Ag66	96	0	12	0	12
H12-C6-O12-Ag67	97	0	29	0	29
H12-C6-O12-Ag68	98	0	16	0	16
H12-C6-O12-Ag72	102	0	1	0	1

H12-C6-O12-Ag88	118	0	30	0	30
H12-C6-O13-Ag58	89	0	6	0	6
H12-C6-O13-Ag59	90	0	2	0	2
H12-C6-O13-Ag62	93	0	3	0	3
H12-C6-O13-Ag63	94	0	3	0	3
H12-C6-O13-Ag66	97	0	10	0	10
H12-C6-O13-Ag67	98	0	18	0	18
H12-C6-O13-Ag71	102	0	30	0	30
H12-C6-O13-Ag72	103	0	18	0	18
H12-C6-O14-Ag63	95	0	5	0	5
H12-C6-O14-Ag67	99	0	17	0	17
H12-C6-O14-Ag71	103	0	33	0	33
H12-C6-O14-Ag72	104	0	18	0	18
H13-O5-Ag12	30	0	40	0	40
H14-O7	21	0	1	808	809
H15-Ag6	21	0	1	0	1
H16-Ag5	21	0	4	0	4
H16-O8	24	0	14	3955	3969
H16-C8-O5-Ag48	77	0	1	0	1
H16-C8-O5-Ag49	78	0	6	0	6
H16-C8-O5-Ag50	79	0	1	0	1
H16-C8-O5-Ag51	80	0	4	0	4
H16-C8-O6-Ag48	78	0	2	0	2
H16-C8-O6-Ag49	79	0	2	0	2
H16-C8-O6-Ag50	80	0	5	0	5
H16-C8-O6-Ag51	81	0	5	0	5
H16-C8-O7-Ag48	79	0	5	0	5
H16-C8-O7-Ag49	80	0	5	0	5
H16-C8-O7-Ag50	81	0	2	0	2
H16-C8-O7-Ag51	82	0	5	0	5
H16-C8-O8-Ag48	80	0	7	0	7
H16-C8-O8-Ag49	81	0	7	0	7
H16-C8-O8-Ag50	82	0	1	0	1
H16-C8-O8-Ag51	83	0	5	0	5
H16-C8-O8-Ag52	84	0	6	0	6
H16-C8-O8-Ag53	85	0	3	0	3
H16-C8-O8-Ag54	86	0	1	0	1
H16-C8-O8-Ag55	87	0	11	0	11
H16-C8-O9-Ag71	104	0	3	0	3
H16-C8-O9-Ag72	105	0	2	0	2
H16-C8-O10-Ag71	105	0	1	0	1
H16-C8-O10-Ag72	106	0	1	0	1
H16-C8-O11-Ag71	106	0	1	0	1
H16-C8-O11-Ag72	107	0	3	0	3
H16-C8-O12-Ag71	107	0	2	0	2
H16-C8-O12-Ag80	116	0	51	0	51
H16-C8-O13-Ag71	108	0	2	0	2
H16-C8-O15-Ag71	110	0	2	0	2
H23-Ag9	32	0	2	0	2
H23-O11-Ag16	50	0	18	325	343
H24-O11-Ag16	51	0	19	167	186
H25-O11-Ag16	52	0	7	127	134
H30-O15	45	124	4	94	222
total	--	570	22543	27018	50131

3. DFT calculations

All DFT calculations are performed using the plane-wave VASP package.[14] The kinetic energy cutoff was set as 450 eV, the electron-ion interaction was represented by the projector-augmented wave (PAW) pseudopotential, and the exchange functional was evaluated with the GGA-PBE.[15] The Monkhorst−Pack k-mesh was 30 times the reciprocal lattice vectors (1/30 $Å^{-1}$) for optimization, and was 40 times the reciprocal lattice vectors (1/40 $Å^{-1}$) for single point calculations based on the optimized geometry, where the final energy is obtained. For all structures, the energy and force were converged to less than 10^{-6} eV and 0.05 eV/Å. The van der Waals interaction was considered by using DFT-D3 method with zero damping.[10,11]

4. The Gibbs free energy computation

In this work, μ_{Ag} is set as the energy of a Ag atom in bulk silver.

For μ_O, it can be calculated from the thermodynamics equation as

$$\mu_O(T,p) = (\mu_{O2}(T,p^0=1bar) + k_B T ln(P_{O2}/p^0)) / 2$$

where $\mu_{O2}(T,p^0)$ is the zero reference state of μ_{O2}. To avoid the use of DFT energy of spin-polarized O_2 molecule, the standard molar enthalpy of formation of Ag_2O (at 298.15 K, $\Delta_f H_m(Ag_2O)$ = -0.323 eV)[16] is then used to determine the μ_{O2}:

$$\mu_{O2}(T,p^0) = (H(Ag_2O) - 2H(Ag) - \Delta_f H_m(Ag_2O)) \times 2 + \Delta\mu_{O2}(T,p^0)$$

where $H(Ag_2O)$ and $H(Ag)$ is the enthalpy of bulk Ag_2O and Ag on 298.15 K, which can be approximated as the ZPE corrected total energies of a Ag_2O and Ag atom in bulk. $\Delta\mu_{O2}(T,p^0)$ item is the chemical potential variation of 1 bar O_2 from 298.15 K (in enthalpy) to T (in free energy), as obtained to be -1.08 eV by thermodynamic equations under typical ethylene epoxidation condition, T = 500 K and 1 bar of O_2.

5. The benchmark of G-NN potential against DFT

Table S2. Benchmark of G-NN potential against DFT for the calculated γ values of 30 low energy surface oxides on Ag(111). Listed data are the stoichiometry of the structure, the *A* value of its surface periodicity, the total number of atoms (Natoms), the energies in NN (E_{NN}) and DFT (E_{DFT}) level, and the difference of NN and DFT energies (E_{NN-DFT}) in the unit of eV and meV/atom.

Stoichiometry	*A*	Natoms	E_{NN} (eV)	E_{DFT} (eV)	E_{NN-DFT} (eV)	E_{NN-DFT} (meV/atom)
Ag5O4	8	41	-131.732	-131.812	0.0799	1.949
Ag7O7	12	62	-200.656	-200.738	0.0814	1.313
Ag5O5	8	42	-136.833	-136.987	0.1537	3.66
Ag8O6	10	54	-174.86	-175.062	0.202	3.741
Ag4O5	8	41	-133.413	-133.542	0.1295	3.159
Ag10O7	12	65	-210.19	-210.302	0.1127	1.734
Ag7O8	12	63	-205.962	-205.911	-0.0512	-0.813
Ag7O7	11	58	-189.102	-189.21	0.1083	1.867
Ag9O5	12	62	-196.298	-196.54	0.2425	3.911
Ag7O6	10	53	-171.645	-171.691	0.0462	0.872
Ag5O4	8	41	-131.196	-131.349	0.1526	3.722
Ag6O7	11	57	-185.731	-185.715	-0.016	-0.281
Ag8O8	12	64	-209.129	-209.232	0.1025	1.602
Ag7O5	10	52	-166.314	-166.358	0.0437	0.84
Ag8O6	12	62	-198.583	-198.713	0.1309	2.111
Ag7O6	10	53	-172.297	-172.277	-0.0205	-0.387
Ag6O6	10	52	-168.95	-169.008	0.058	1.115
Ag7O6	11	57	-183.955	-184.079	0.1245	2.184
Ag9O6	12	63	-201.756	-202.092	0.3356	5.327
Ag7O6	12	61	-195.214	-195.457	0.2432	3.987
Ag9O7	12	64	-207.168	-207.163	-0.0056	-0.087
Ag8O5	10	53	-169.511	-169.793	0.2813	5.308
Ag7O7	10	54	-177.157	-177.118	-0.0391	-0.724
Ag8O7	12	63	-203.867	-204.015	0.1487	2.36
Ag5O6	10	51	-165.266	-165.316	0.0504	0.988
Ag10O6	12	64	-204.873	-204.994	0.1214	1.897
Ag8O6	11	58	-186.8	-186.971	0.1702	2.934
Ag7O5	11	56	-178.286	-178.422	0.1364	2.436
Ag6O7	10	53	-174.041	-173.957	-0.0842	-1.589
Ag8O4	10	52	-164.151	-164.338	0.1872	3.6

Table S3. Benchmark of G-NN potential against DFT for the calculated γ values of 30 low energy surface oxides on Ag(100). Listed data are the stoichiometry of the structure, the *A* value of its surface periodicity, the total number of atoms (Natoms), the energies in NN (E_{NN}) and DFT (E_{DFT}) level, and the difference of NN and DFT energies (E_{NN-DFT}) in the unit of eV and meV/atom.

Stoichiometry	*A*	Natoms	E_{NN} (eV)	E_{DFT} (eV)	E_{NN-DFT} (eV)	E_{NN-DFT} (meV/atom)
Ag7O5	8	44	-141.716	-141.844	0.1283	2.916
Ag7O6	10	53	-169.997	-170.059	0.0625	1.179
Ag8O6	9	50	-161.766	-161.906	0.1398	2.796
Ag9O6	12	63	-199.526	-199.643	0.1173	1.862
Ag9O6	12	63	-199.524	-199.612	0.0878	1.394
Ag4O4	5	28	-92.1264	-92.0762	-0.0502	-1.793
Ag8O8	10	56	-184.263	-184.167	-0.0951	-1.698
Ag10O7	11	61	-196.438	-196.581	0.1438	2.357
Ag9O6	12	63	-199.452	-199.475	0.0227	0.36
Ag10O8	12	66	-213.473	-213.69	0.2168	3.285
Ag3O2	4	21	-66.5331	-66.5875	0.0544	2.59
Ag6O4	8	42	-133.052	-133.173	0.1213	2.888
Ag6O4	8	42	-132.86	-132.927	0.0669	1.593
Ag10O6	12	64	-202.659	-202.803	0.1445	2.258
Ag10O8	12	66	-213.473	-213.667	0.1942	2.942
Ag10O7	12	65	-208.112	-208.459	0.3472	5.342
Ag8O7	12	63	-201.647	-201.801	0.1533	2.433
Ag6O6	10	52	-166.898	-167.001	0.1032	1.985
Ag7O6	10	53	-169.987	-170.094	0.1069	2.017
Ag10O7	11	61	-196.445	-196.628	0.1826	2.993
Ag6O4	7	38	-121.493	-121.638	0.145	3.816
Ag3O2	4	21	-66.5241	-66.5606	0.0365	1.738
Ag10O7	12	65	-207.908	-208.172	0.2637	4.057
Ag6O4	7	38	-121.489	-121.613	0.1241	3.266
Ag8O6	9	50	-161.73	-161.922	0.1916	3.832
Ag9O6	12	63	-199.441	-199.495	0.0538	0.854
Ag10O8	12	66	-213.487	-213.701	0.2146	3.252
Ag6O4	8	42	-132.845	-132.928	0.0833	1.983
Ag10O6	12	64	-202.65	-202.772	0.1216	1.9
Ag6O4	8	42	-133.042	-133.095	0.0523	1.245

The benchmark of G-NN potential against DFT is conducted by comparing the γ values of low energy 30 surface oxides on Ag(111) and Ag(100) with those calculated by DFT. The data can be found in Table S2 and S3, in which the maximum and root mean square (RMS) errors for the energy of surface oxides on Ag(111) are 5.327 and 2.627 meV/atom, while that on Ag(100) are 5.342 and 2.635 meV/atom, respectively.

6. The PES contour map construction

To construct the PES map, we utilized the Gaussian smearing method to map discrete grid points to a continuous contour plot. This is demonstrated in the following for Ag(111). Figure S1 left shows the data obtained from the phase database after the ASOP simulation, where each point corresponds to one composition with the specified Ag and O coverage and the color represents its γ value (the lowest γ value of the composition from the phase database). For each point, a Gaussian smearing with σ=0.1 (0.1 ML) is conducted for 2D-interpolation, see Eq. (9) in the main text. This will yield the smeared value for neighboring grid points. The final γ value for each point is then obtained using Eq. (8) in the main text, i.e. the lowest value from all smeared values at this point.

By this method, the γ value for local minima will not be affected and the value for other neighboring points may be reduced. To estimate the error of smearing, we have compared the γ value of four compositions in the database (real) and in the PES map (smear), as shown in Figure S1. For the optimal phase (point 1) or the metastable phase locates in the high energy zone (point 2), both being local minima on PES, there are no errors after smearing. The smearing errors are present for the points adject to the local minima, such as point 3 and 4, where the smearing lowers their γ values depending on the stability of the adjacent composition and the distance.

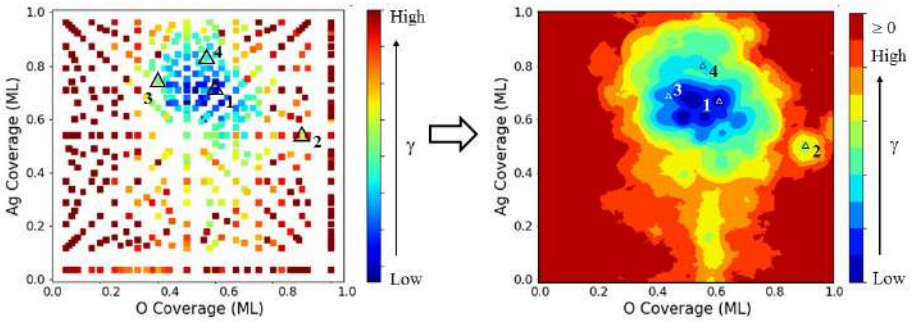

Point	γ (real)	γ (smear)
1	-0.29	-0.29
2	-0.13	-0.13
3	-0.15	-0.22
4	-0.17	-0.20

Figure S1. The process of PES smearing for surface oxides on Ag(111), which maps the discrete data from the phase database (left) to the contour pot (right, see also in Figure 4). The γ values of four compositions (1 ~ 4) in the database (real) and in the smearing PES map (smear) are also listed for comparison.

7. The geometries of surface oxides with the increasing of O coverage

Table S4. The geometries of optimal surface oxides in A = 8 with the specified O coverage (from O1 to O8) on Ag(111) and Ag(100).

Ag(111)	O coverage	Ag(100)
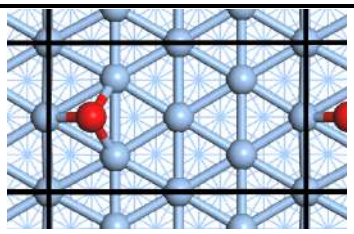 O_1	0.125 ML	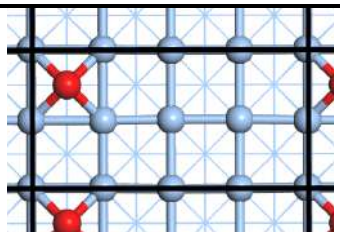 O_1
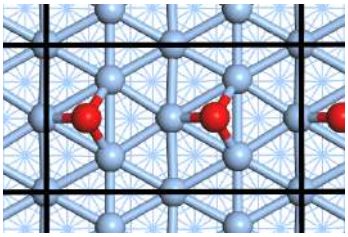 O_2	0.250 ML	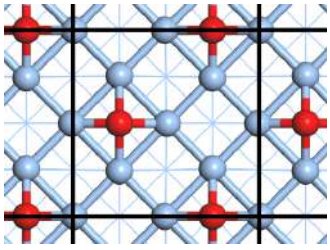 O_2
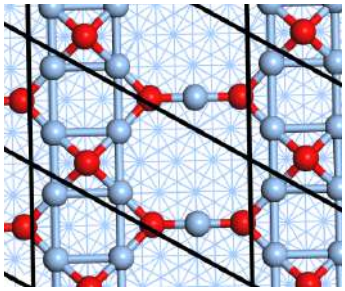 Ag_5O_3	0.375 ML	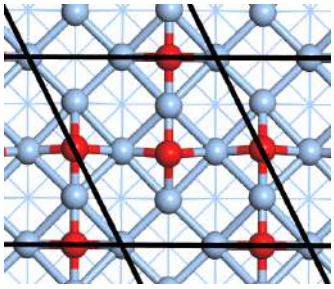 O_3
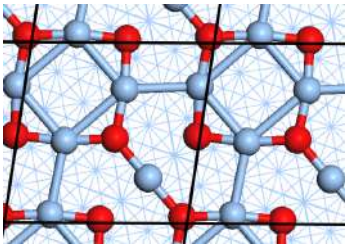 Ag_5O_4	0.500 ML	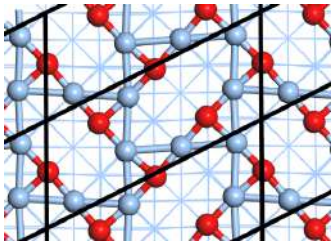 Ag_6O_4
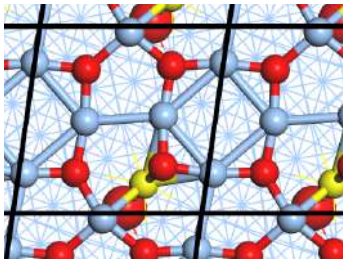 Ag_5O_5	0.625 ML	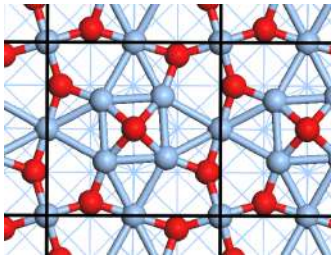 Ag_7O_5

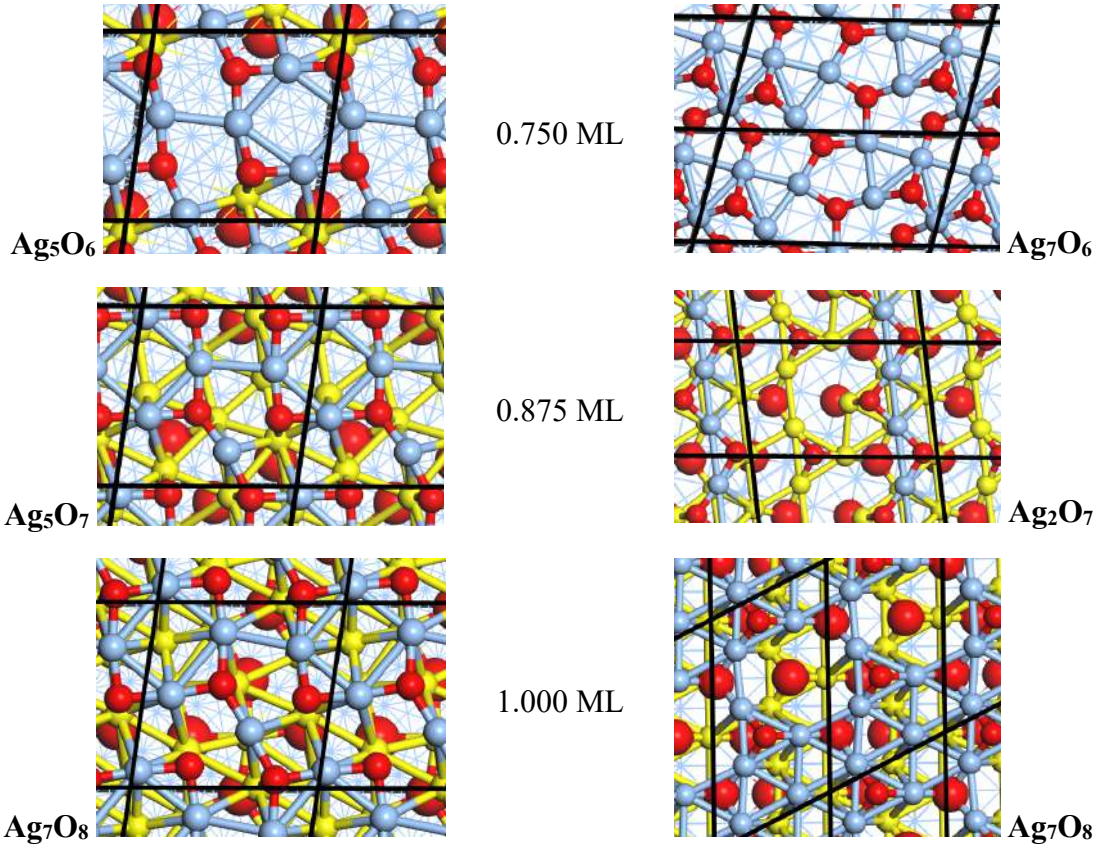
Ag5O6
0.750 ML
Ag7O6
Ag5O7
0.875 ML
Ag2O7
Ag7O8
1.000 ML
Ag7O8

References

[1] S.-D. Huang, C. Shang, X.-J. Zhang, and Z.-P. Liu, Chem. Sci. **8**, 6327 (2017).
[2] S.-D. Huang, C. Shang, P.-L. Kang, and Z.-P. Liu, Chem. Sci. **9**, 8644 (2018).
[3] C. Shang, S.-D. Huang, and Z.-P. Liu, J. Comput. Chem. **40**, 1091 (2019).
[4] C. Shang and Z.-P. Liu, J. Chem. Theory Comput. **9**, 1838 (2013).
[5] X.-J. Zhang, C. Shang, and Z.-P. Liu, J. Chem. Theory Comput. **9**, 3252 (2013).
[6] C. Shang, X.-J. Zhang, and Z.-P. Liu, Phys. Chem. Chem. Phys. **16**, 17845 (2014).
[7] C. Shang and Z.-P. Liu, J. Chem. Theory Comput. **8**, 2215 (2012).
[8] S.-D. Huang, C. Shang, P.-L. Kang, X.-J. Zhang, and Z.-P. Liu, WIREs Comput. Mol. Sci. **9**, e1415 (2019).
[9] S. Ma, C. Shang, and Z.-P. Liu, J. Chem. Phys. **151**, 050901 (2019).
[10] S. Grimme, S. Ehrlich, and L. Goerigk, J. Comput. Chem. **32**, 1456 (2011).
[11] S. Grimme, J. Antony, S. Ehrlich, and H. Krieg, J. Chem. Phys. **132**, 154104 (2010).
[12] M. Schmid, A. Reicho, A. Stierle, I. Costina, J. Klikovits, P. Kostelnik, O. Dubay, G. Kresse, J. Gustafson, E. Lundgren, J.N. Andersen, H. Dosch, and P. Varga, Phys. Rev. Lett. **96**, 146102 (2006).
[13] D. Chen, P.-L. Kang, and Z.-P. Liu, ACS Catal. **11**, 8317 (2021).
[14] G. Kresse and J. Furthmüller, Phys. Rev. B **54**, 11169 (1996).
[15] J.P. Perdew, K. Burke, and M. Ernzerhof, Phys. Rev. Lett. **77**, 3865 (1996).
[16] R.D. Lide, *CRC Handbook of Chemistry and Physics*, 95th ed. (CRC Press, New York, 2015).

8. XYZ coordinates for the stable silver surface oxides shown in Figure 4(b) and Figure 5(b)

Here, all of these structures are provided in VASP POSCAR format.

(1) Ag_5O_4 on (√7×√7)R19 of Ag(111)

```
Structure
 1.00000000
   7.62640   0.00000   0.00000
   1.08948   7.54818   0.00000
  -0.00000  -0.00000  25.09070
   H    C    O    Ag
   0    0    4   37
 D
    0.518931    0.018669    0.486526
    0.968018    0.034751    0.496270
    0.985051    0.484182    0.485680
    0.534633    0.468550    0.497653
    0.125000    0.625000    0.119566
    0.375001    0.875000    0.119566
    0.000000    0.000000    0.119566
    0.250000    0.250000    0.119566
    0.500000    0.500000    0.119566
    0.750000    0.750000    0.119566
    0.625000    0.125000    0.119566
    0.875000    0.375000    0.119566
    0.083332    0.416667    0.213368
    0.333332    0.666667    0.213368
    0.583332    0.916667    0.213368
    0.208332    0.041666    0.213368
    0.458332    0.291666    0.213368
    0.708332    0.541667    0.213368
    0.958332    0.791667    0.213368
    0.833332    0.166666    0.213368
    0.040549    0.209091    0.307707
    0.791030    0.959577    0.307717
    0.541254    0.705558    0.306969
    0.294556    0.458748    0.306912
    0.418544    0.083401    0.306541
    0.669006    0.331005    0.310267
    0.916562    0.581461    0.306504
    0.163732    0.836330    0.306685
    0.260970    0.454025    0.494104
    0.880505    0.378681    0.403851
    0.504713    0.495903    0.403248
    0.242308    0.048450    0.493867
    0.252269    0.249863    0.398302
    0.372582    0.871220    0.398076
    0.954254    0.760545    0.493665
```

0.128789 0.627341 0.397915
0.750680 0.748141 0.398295
0.750147 0.250721 0.500139
0.548658 0.742463 0.494268
0.621431 0.119517 0.403838
0.996656 0.004045 0.402424

(2) $Ag_{10}O_9$ on (2√7×√7)R19 of Ag(111)

Structure
1.00000000
7.61370 0.00000 0.00000
2.17534 15.07122 0.00000
-0.00000 -0.00000 25.04880
H C O Ag
0 0 9 74
D
0.507350 0.509545 0.516078
0.037602 0.761639 0.490297
0.458144 0.259003 0.499372
0.481029 0.985581 0.487480
0.051384 0.484392 0.494215
0.029477 0.986056 0.498553
0.007606 0.261489 0.491618
0.483156 0.779003 0.493006
0.336356 0.387169 0.383017
0.125000 0.812498 0.119766
0.375000 0.937498 0.119766
0.000000 0.499999 0.119766
0.250000 0.624998 0.119766
0.499999 0.749998 0.119766
0.749999 0.874998 0.119766
0.125000 0.312499 0.119766
0.374999 0.437499 0.119766
0.624999 0.562499 0.119766
0.874998 0.687498 0.119766
0.000000 0.000000 0.119766
0.249999 0.125000 0.119766
0.499999 0.249999 0.119766
0.749998 0.374999 0.119766
0.624998 0.062500 0.119766
0.874998 0.187500 0.119766
0.083332 0.708331 0.213568
0.333332 0.833331 0.213568
0.583331 0.958331 0.213568
0.208332 0.520832 0.213568
0.458331 0.645832 0.213568
0.708330 0.770831 0.213568

0.958330 0.895831 0.213568
0.083332 0.208333 0.213568
0.333331 0.333332 0.213568
0.583331 0.458332 0.213568
0.833330 0.583332 0.213568
0.208331 0.020833 0.213568
0.458331 0.145833 0.213568
0.708330 0.270833 0.213568
0.958330 0.395832 0.213568
0.833330 0.083333 0.213568
0.168385 0.915310 0.310891
0.919421 0.791910 0.306870
0.540704 0.854789 0.307397
0.288106 0.228074 0.307125
0.415500 0.040390 0.306781
0.044615 0.603781 0.307271
0.291505 0.729427 0.308408
0.661104 0.168131 0.306590
0.039612 0.102577 0.307417
0.794127 0.979383 0.306936
0.164014 0.417109 0.306336
0.419437 0.540717 0.307571
0.665730 0.668393 0.306979
0.542656 0.354716 0.307813
0.915851 0.291960 0.307805
0.794745 0.479710 0.307689
0.881661 0.684843 0.399021
0.011312 0.497029 0.402086
0.729923 0.270893 0.496783
0.474520 0.644378 0.500893
0.110679 0.305000 0.404943
0.755068 0.874704 0.398175
0.868286 0.184814 0.399072
0.420037 0.454663 0.447494
0.748474 0.376966 0.401761
0.636913 0.565279 0.399655
0.757221 0.975825 0.495190
0.263498 0.621689 0.400244
0.628038 0.062865 0.398289
0.247720 0.122462 0.399308
0.004474 0.997031 0.404308
0.498599 0.246604 0.403056
0.760307 0.778484 0.494715
0.220757 0.356642 0.508722
0.449517 0.123160 0.495218
0.064295 0.622720 0.495701
0.381809 0.938373 0.403391
0.126271 0.808821 0.405621
0.778779 0.489209 0.501456
0.502973 0.752081 0.401621
0.254410 0.881261 0.502035

0.042308 0.122690 0.496611

(3) $Ag_{12}O_6$ on p(4×4) of Ag(111)

Structure
1.00000000
11.53000 0.00000 0.00000
-5.76500 9.98527 0.00000
-0.00000 -0.00000 25.09070
H C O Ag
0 0 6 76
D
0.378972 0.750909 0.522177
0.998752 0.428082 0.489085
0.676531 0.751898 0.488712
0.321744 0.073870 0.489662
0.620660 0.373400 0.523687
0.998995 0.130600 0.523422
0.000000 0.000000 0.119566
0.250001 0.000000 0.119566
0.500001 0.000000 0.119566
0.750002 0.000000 0.119566
0.000000 0.250001 0.119566
0.250001 0.250001 0.119566
0.500001 0.250001 0.119566
0.750002 0.250001 0.119566
0.000000 0.500001 0.119566
0.250001 0.500001 0.119566
0.500001 0.500001 0.119566
0.750002 0.500001 0.119566
0.000000 0.750002 0.119566
0.250001 0.750002 0.119566
0.500001 0.750002 0.119566
0.750002 0.750002 0.119566
0.083477 0.166140 0.213862
0.332554 0.166020 0.213890
0.582648 0.167027 0.213897
0.833982 0.167419 0.213828
0.083118 0.417571 0.213860
0.333363 0.416998 0.213356
0.584007 0.417757 0.213844
0.833631 0.417817 0.213939
0.083532 0.667595 0.215308
0.332534 0.666975 0.213914
0.584292 0.667249 0.213889
0.833794 0.666708 0.215319
0.082717 0.916479 0.215456
0.332323 0.916298 0.213984

0.583177	0.916227	0.213797
0.834009	0.916549	0.213951
0.167164	0.084277	0.308383
0.415374	0.082536	0.307108
0.666656	0.084309	0.306042
0.916873	0.082855	0.306581
0.166871	0.334703	0.305781
0.416094	0.334061	0.305799
0.667675	0.335501	0.306563
0.915895	0.334893	0.306954
0.166399	0.583832	0.308249
0.417150	0.584336	0.305891
0.666588	0.584627	0.308249
0.918192	0.584306	0.309137
0.166580	0.835334	0.309222
0.415701	0.834428	0.306755
0.668248	0.835170	0.307052
0.915313	0.832706	0.309283
0.000178	0.000204	0.402457
0.249983	0.000644	0.403070
0.500616	0.999169	0.400003
0.752511	0.004396	0.399863
0.000505	0.250950	0.397493
0.247848	0.251983	0.400232
0.499676	0.251719	0.397528
0.747055	0.251294	0.399839
0.999806	0.500883	0.402623
0.252967	0.502997	0.399987
0.498867	0.498113	0.400119
0.750679	0.502194	0.402192
0.000098	0.750926	0.404610
0.249250	0.750958	0.402239
0.499656	0.750699	0.397712
0.750348	0.751429	0.402600
0.666513	0.568203	0.503309
0.422078	0.584381	0.493241
0.183043	0.601257	0.503038
0.165409	0.339596	0.493148
0.815660	0.419308	0.503504
0.576803	0.163845	0.492758
0.410864	0.328033	0.493280
0.148217	0.083917	0.504043
0.833592	0.174989	0.492673
0.332743	0.900525	0.503329
0.850029	0.935421	0.503315
0.588888	0.918741	0.492775

(4) Ag_7O_5 on $(2\sqrt{2}\times2\sqrt{2})R45^o$ of Ag(100)

Structure
1.00000000
8.15300 0.00000 0.00000
-0.00000 8.15300 0.00000
-0.00000 -0.00000 24.14480
H C O Ag
0 0 5 39
D
0.175264 0.253603 0.469880
0.502124 0.077399 0.469471
0.325450 0.750069 0.469893
0.750343 0.501762 0.514748
0.998494 0.926381 0.469855
0.000000 0.749996 0.124250
0.000000 0.249999 0.124250
0.249999 0.499998 0.124250
0.499998 0.749996 0.124250
0.249999 0.000000 0.124250
0.499998 0.249999 0.124250
0.749996 0.499998 0.124250
0.749996 0.000000 0.124250
0.000000 0.499998 0.208668
0.249999 0.749996 0.208668
0.000000 0.000000 0.208668
0.249999 0.249999 0.208668
0.499998 0.499998 0.208668
0.749996 0.749996 0.208668
0.499998 0.000000 0.208668
0.749996 0.249999 0.208668
0.499953 0.250521 0.294408
0.000186 0.250191 0.294421
0.499551 0.750689 0.294228
0.750060 0.500222 0.294454
0.249978 0.500279 0.294432
0.000411 0.750787 0.294299
0.250033 0.000301 0.294398
0.750016 0.000200 0.294391
0.250436 0.750140 0.378642
0.997378 0.506657 0.379674
0.756128 0.253905 0.379399
0.250388 0.002026 0.480583
0.250127 0.251834 0.378519
0.750421 0.002326 0.470205
0.936456 0.337421 0.483694
0.913198 0.688388 0.483813
0.500686 0.000632 0.378379
0.999659 0.000670 0.378478
0.744378 0.748191 0.379410
0.586694 0.315641 0.483402
0.564132 0.665821 0.483807
0.250460 0.501791 0.470471

0.502796 0.495856 0.379595

(5) Ag_3O_2 on (2√2×√2)R45° of Ag(100)

Structure
1.00000000
4.07650 0.00000 0.00000
-0.00000 8.15300 0.00000
-0.00000 -0.00000 24.14480
H C O Ag
0 0 2 19
D
0.999182 0.992528 0.479239
0.001144 0.506733 0.479283
0.000000 0.749996 0.124250
0.000000 0.249999 0.124250
0.499998 0.499998 0.124250
0.499998 0.000000 0.124250
0.000000 0.499998 0.208668
0.499998 0.749996 0.208668
0.000000 0.000000 0.208668
0.499998 0.249999 0.208668
0.500198 0.001471 0.294164
0.000230 0.749643 0.293334
0.000213 0.249756 0.295403
0.500278 0.498090 0.294173
0.499413 0.965271 0.469300
0.000099 0.996064 0.378565
0.000285 0.502525 0.378596
0.500121 0.249270 0.381447
0.000175 0.249388 0.473810
0.500548 0.535162 0.469789
0.500355 0.749204 0.376246